PCCP

Accepted Manuscript

ROYAL SOCIETY OF CHEMISTRY

www.rsc.org/pccp

Characterization of Molecular Association of Poly(2-oxazoline)s-based Micelles with Various Epoxides and Diols via the Flory-Huggins Theory: A Molecular Dynamics Simulation Approach

Byeong Jae Chun,[1,2] Jie Lu,[3] Marcus Weck,[3] and Seung Soon Jang[2,4,5*]

[1] School of Chemical & Biomolecular Engineering, Georgia Institute of Technology, 311 Ferst Drive NW, Atlanta, Georgia 30332-0100, USA

[2] Computational NanoBio Technology Laboratory, School of Materials Science and Engineering, Georgia Institute of Technology, 771 Ferst Drive NW, Atlanta, Georgia 30332-0245, USA

[3] Department of Chemistry, New York University, 100 Washington Square East, New York, New York 10003, USA

[4] Institute for Electronics and Nanotechnology, Georgia Institute of Technology, Atlanta, GA, USA

[5] Parker H. Petit Institute for Bioengineering and Bioscience, Georgia Institute of Technology, Atlanta, GA, USA

[*] To whom correspondence should be addressed.
Professor Seung Soon Jang, E-mail: SeungSoon.Jang@mse.gatech.edu

ABSTRACT

The hydrolytic kinetic resolution (HKR) of epoxides has been performed in a shell-crosslinked micellar (SCM) nanoreactor consisting of amphiphilic triblock copolymers based on poly(2-oxazline)s polymer derivatives with attached Co (III)-salens to the micelle core. To investigate the effect of the molecular interaction of reactant/product molecules with the SCM nanoreactor on the rate of HKR, we calculated the Flory-Huggins interaction parameters (χ) using the molecular dynamics simulation method. For this, the blend systems were constructed with various compositions such as 15, 45, and 70 wt% of the reactant/product molecules with respect to the polymers such as poly(2-methyl-2-oxazoline) (PMOX), poly(2-(3-butinyl)2-oxazoline) (PBOX), and poly(methyl-3-(oxazol-2-yl) pentanoate with Co(III)-salen (PSCoX). From the χ parameters, we demonstrate that the miscibility of reactants/products with polymers has a strong correlation with the experimental reaction rate of the HKR: phenyl glycidyl ether (Reac-OPh) > epoxyhexane (Reac-C4) > styrene oxide (Reac-Ph) > epichlorohydrin (Reac-Cl). To validate this finding, we also conducted the potential of mean force analysis using steered molecular dynamics simulation for the molecular displacement of Reac-Cl and Reac-OPh through PMOX and PSCoX, revealing that the free energy reduction was greater when Reac-OPh molecule enters the polymer phase compared to Reac-Cl, which agrees with the findings from the χ parameters calculations.

Keywords: hydrolytic kinetic resolution, multicompartment micelle, molecular dynamics simulation, Flory-Huggins interaction parameter

1. Introduction

Micelles consisting of poly(2-oxazoline)s (POXs) block copolymers have been extensively studied due to their potential for a variety of applications[1, 2] including drug delivery,[3, 4] pharmaceutical applications,[5, 6] and catalysis.[7-9] This variety of applications is attributed to the two aspects of POXs block copolymers: 1) the micelle properties that can be easily tuned by designing polymer blocks[1, 2, 10] and 2) the chain architectures of POXs block copolymer that can be tailor-made using living cationic ring-opening polymerization.[1, 2, 11-19]

Among the applications mentioned above, we focus on micellar catalysis.[2, 7, 9, 20, 21] An exceptional catalytic environment within a micelle structure can be created via well-defined phase-segregated internal structure of the micelle assemblies.[7-9] Commonly, the embedment of a catalyst into the core compartment of the micelle forms a high concentration of catalysts within the given volume of the micelle core, which provides a favorable condition for catalytic reactions.[8, 9] This idea can be expanded further to obtain consecutive reactions through the neighboring compartments in a micelle or through the combined multiple micelles.[8]

We have reported that the hydrolytic kinetic resolution (HKR) of epoxides can be performed in nanoreactors consisting of POXs-based shell cross-linked multicompartment micelle (SCM) and Co (III)-salen complex.[8] Kinetic resolution is a process in which one enantiomer reacts significantly faster than the other, leading to an accumulation of the less reactive enantiomer.[22, 23] By this, diol product will be produced from epoxide reactant due to the decisive difference in reaction kinetics. In this study, our simulation will focus on the diol molecule only because it is the main product. The core domain of the micelles containing Co (III)-salen is a highly reactive site due to its high catalyst concentration. The epoxide of interest (reactant) diffuses into the micelle core due to its hydrophobicity, while the hydrophilic diol product from HKR is released into the surrounding aqueous phase due to its hydrophilicity. Despite our success in developing a highly efficient micelle-based nanoreactor, we were not able to explain why the HKR for certain types of epoxide (e.g., epichlorohydrin) in the SCM does not occur or is very slow in comparison to the HKR in the bulk phase.[24] This contribution investigates the relationship of the properties for reactant/product with the characteristics of HKR catalyzed by the SCM nanoreactor.

Molecular simulation methods have been widely applied to investigate molecular properties based on their chemical structures.[25, 26] Particularly, molecular simulations have

been extensively performed to study drug-polymer compatibility[27-31] and the drug release properties of drug carriers:[32-37] the former is determined by obtaining the thermodynamic properties such as free energy, whereas the latter describes kinetic properties related to molecular transport with energy barriers.

The focus of the present study is to predict the compatibility of reactant/product molecules with a POX-based block copolymer. In the aforementioned studies on the drug-polymer compatibility,[27-30, 38] the quantitative evaluation of such compatibility was attempted by employing the Flory-Huggins interaction parameters (χ). Patel and his coworkers[23] reported molecular dynamics (MD) simulations investigating the compatibility between water-insoluble drugs and self-associating PEO-b-PCL block copolymers. Kasimova *et al.*[39] performed MD simulations of lipophlilic drug molecules in polymeric micelles, which was validated by experiments. Both studies employed the χ parameters as a descriptor for phase segregation or miscibility, which could establish a systematic design guide in efficiently developing new drugs with less use of resources.

We have reported that the reaction kinetics of HKR of epoxides depend on the chemical structure of reactant and product in the POXs block copolymer micelles.[8] Based on these results, we hypothesize that the compatibility of reactant/product with the POXs-based block copolymer has a significant influence on the kinetics through the molecular transport since the reactant may not enter the micelle if the compatibility is low, and similarly, the product will stay in the micellar core if the compatibility is high.

In this study, we characterize the compatibility of various reactant/product molecules with each block of POXs-based block copolymer by calculating the χ parameter from MD simulations, in order to investigate the effect of the compatibility on the reaction. Our simulation results are compared to the corresponding experimental observation.

2. Materials and Simulation Methods

2.1. Simulated Materials

The crosslinked micelle is formed from amphiphilic ABC-triblock copolymers based on poly(2-oxazoline)s. The polymer has a hydrophilic block (A) and a hydrophobic block (C). To stabilize the micelle, a crosslinking block (B) is introduced into the middle layer of the polymer. Monomer C was synthesized following the literature procedure[40] while monomer B was synthesized by a two-step one-pot reaction with a yield of 72% (see SI). Poly(2-

oxazoline) triblock copolymers were synthesized via cationic ring-opening polymerization using methyl triflate as the initiator. The polymerization process was monitored by ^{1}H NMR spectroscopy and gel-permeation chromatography (GPC). The dispersity (*Đ*) and apparent molecular weight (M_n^{app}) of the final triblock copolymer **1** are 1.23 and 7,700 g mol^{-1} respectively, as determined by gel-permeation chromatography using poly(styrene) standards (see SI). ^{1}H NMR spectrum of **1** showed degrees of polymerization of the individual blocks of a:b:c=62.1:6.7:8.3 (see SI). The ester end groups in the side-chain of hydrophobic block C were deprotected into carboxylic acids and served as a functional handle to attach the hydroxyl-functionalized salen ligand. The MALDI-TOF spectrum indicated that four salen ligands were attached in the hydrophobic block of polymer **2** (see SI). Micelle formation was induced by dissolving polymer **3** in water (5 mg/mL) and was proved by dynamic light scattering (DLS) analysis. The thiol-yne reaction was chosen for the micelle crosslinking step between a dithiol linker and the carbon-carbon triple bonds in block B. The stable hydrodynamic radius from DLS analysis in different solvents proved the success of crosslinking. The SCMs were metalated with cobalt(II) acetate in a glovebox and then oxidized in air to produce the active Co(III)-salen micelles **5** (Scheme 1). The hydrodynamic radius of **5**, determined by DLS, was 47 ± 5 nm, consistent with the radius of 50 ± 10 nm obtained by SEM (see SI). We studied the use of **5** as catalyst for the HKR of epoxides. Table 1 shows the reactants and corresponding products for the HKR using **5** with detailed information on reaction times and conversions. The conversion of HKR reaction was determined by chiral GC measurement. The chirality of the salen ligand only allows one enantiomer to reach the cobalt metal while the other enantiomer cannot be catalyzed due to the steric hindrance. Therefore, the highest conversion of a kinetic resolution reaction is 50 %. After 24 h, epichlorohydrin (entry 1) was less than 4% converted with an *ee* of 5%. Stryene oxide (entry 2) reached 48% conversion and 92% *ee* after twelve hours. Epoxyhexane (entry 3) with a longer side chain was completed in twelve hours with 96% *ee*. Phenyl glycidyl ether was resolved in five hours with 95% *ee*. These catalytic results using **5** were in agreement with our previous reported SCM catalysts.[8] Figure 2 shows the structures of reactants and products.

For the computations, we investigate three polymer blocks: poly(2-methyl-2-oxazoline) (PMOX), poly(2-(3-butinyl)-2-oxazoline) (PBOX), and poly(methyl-3-oxazol-2-yl) pentanoate with Co(III)-salen (PSCoX) as shown in Figures 1a, 1b and 1c, respectively.

The POXs block copolymers containing these blocks form micelles in aqueous condition, as observed experimentally. Co-Salen in Figure 1c is Co(III)-salen (Figure 1d). To obtain the compatibility of reactants/products with each block, we modeled each block separately without other blocks, meaning that we performed MD simulations of the three types of homopolymers to investigate their molecular miscibility with the reactants and products in HKR.

2.2. Flory-Huggins Interaction Parameters (χ_{FH}) for Molecule-Polymer Interactions

The Flory-Huggins (FH) interaction Parameters (χ_{FH}) is employed to evaluate the miscibility of reactants and products with each block, which is defined by the following equation:[29]

$$\chi_{FH} = \frac{V_{ref}\,\Delta H_{mix}}{RT} \quad (1)$$

where V_{ref} is the molar volume of molecules in the mixture systems and ΔH_{mix} denotes the enthalpy of mixing, a measure of the molecular interaction. The phase separation becomes greater as a function of χ_{FH} parameter.

In numerous studies,[28-30, 38] the χ_{FH} has been used to characterize the interactions in drug-polymer binary systems. Originally, the FH theory was developed based on the lattice system to investigate the mixiFng of polymeric binary system using the Gibbs free energy change:[25]

$$\Delta G_{mix} = RT\,[n_1 \ln \varphi_1 + n_2 \ln \varphi_2 + n_1 \varphi_2 \chi_{FH}] \quad (2)$$

where R is the gas constant, T is the absolute temperature (K), and n_i and φ_i denote the number of moles and the volume fraction, respectively. The first two terms express the entropy of mixing while the last term describes the enthalpy of mixing. The dimensionless χ_{FH} parameter describes the interaction between reactant/product and polymer.

Recently, there have been several studies[28-30, 38] presenting the calculation of χ_{FH} through MD simulations. We calculated ΔE_{mix} from the energy of binding (ΔE_{bind}) of

pure molecules (component 1), pure polymers (component 2), and molecule-polymer mixture (component 1-2) as Kasimova *et al*.[29] implemented in their work:

$$\Delta E_{mix} = \varphi_1 \left(\frac{\Delta E_{bind}}{V} \right)_1 + \varphi_2 \left(\frac{\Delta E_{bind}}{V} \right)_2 - \left(\frac{\Delta E_{bind}}{V} \right)_{1-2} \quad (3)$$

where φ_1 and φ_2 are the volume fractions of components 1 and 2 in the mixture, V is the total volume of the system. Accordingly, the energy of mixing is dependent of the volume fraction of components in the mixture system, meaning that three systems should be simulated independently to calculate one χ_{FH} for a molecule-polymer pair. All the parameters in Equation (3) are directly taken from the trajectory of MD simulation.

2.3. DFT and MD Simulation Approach

The POX homopolymers were simulated using a full-atomistic model with the Dreiding force field.[41] The atomic partial charges for the repeating units were calculated using Mulliken population[42] with B3LYP/6-31G** in Jaguar.[43]

The temperature was maintained using Nosé-Hoover thermostat.[44, 45] The particle-particle particle-mesh (PPPM) method was used for the long-range electrostatic interaction calculation.[46] The equation of motion was integrated using velocity-Verlet algorithm with a time step of 1 fs.[47] A periodic boundary condition was imposed in all directions. The LAMMPS (large-scale atomic/molecular massively parallel simulator) code developed by Sandia National Laboratories was employed to perform MD simulations.[48]

3. Results and Discussion

3.1. Evaluation of hydrophilicity and hydrophobicity

The solvation free energy of each block was estimated via DFT calculation, which represents the extent of solvation in water. It is noted that the DFT-based solvation free energy has been widely used to indirectly evaluate the solubility of various molecules in a certain implicit solvent phase with a very dilute condition.[24]

On the other hand, MD simulation can describe relatively high concentration condition using explicit solvent method, and thereby take into account the effect of other molecules including the solvent molecules on the molecular structure and dynamics. Thus, the molecular aggregate in water may undergo structural change over a certain period of the

simulation time, depending on the molecular interaction with water phase, which cannot be fully considered in the implicit solvent method. We presume that, if we start MD simulation of molecular aggregate in water phase, the hydrophilic molecular aggregate would become dispersed, whereas the hydrophobic molecular aggregate would be maintained to minimize the contact with the aqueous phase. Based on this, the proposed work was performed in an attempt to assess a relative degree of hydrophobicity of blocks through the structural evolution in water phase in MD simulation.

Solvation Free Energy from DFT Calculations. We used oligomers to model each block as shown in Figure 3 although each block has much longer length with higher degree of polymerization in the experimental work. Here, for fair comparison, we need to adjust the degree of polymerization (DP) to have similar molecular surface area that determines the amount of interaction with the surrounding water molecules. The Co(III)-salen attached with methyl 3-(oxazol-2-yl) pentanoate (hereinafter SCoX) has a molecular surface area of 262.45 $Å^2$, so that an octamer of 2-methyl-2-oxazoline (hereinafter MOX) and a tetramer of 2-(-3-butinyl)-2-oxazoline (hereinafter BOX) were prepared to have the molecular surface area of 238.35 $Å^2$ and 237.49 $Å^2$, respectively, as summarized in Table 2 and Figure 3, in order to eliminate the effect of molecular surface area.

The solvation free energy of an octamer of MOX, tetramer of BOX, and SCoX were estimated to be -50.28 kcal/mol, -42.60 kcal/mol, and -32.96 kcal/mol, respectively, via DFT calculation. The results showed that the octamer of MOX is the most soluble in water whereas the organic complex of SCoX is the least soluble. This assessment agrees with the expectation of the hydrophilicity rank along the block copolymer for micelle formation in the experiment, which consists of PMOX, PBOX, and PSCoX for corona block, intermediate block, and core block, respectively (hereinafter PMOX, PBOX, and PSCoX) .

Change in Radius of Gyration from Molecular Dynamics Simulations. The clusters of homo-oligomers in water phase were monitored during equilibration at 300 K and 1 atm via NPT-MD simulation. As performed in the DFT calculation, since the size of two monomers, MOX and BOX, is far smaller than the size of SCoX, decamers of MOX and BOX were built to prepare clusters while a single unit of SCoX was used to prepare its cluster. The details of the simulation conditions are introduced in Table 3. The initial aggregates were prepared in vacuum, and then the rest of the space in the simulation box was filled with water molecules. In the beginning of the simulation, the restrained MD simulations were performed for 2 ns in

order to relax the system, especially the aggregates-water interface as well as the water phase. Then, the MD simulations were performed to investigate the change in the radius of gyration (R_g) of the aggregates. Figure 4 shows that the radius of gyration of the MOX-decamer aggregate (Figure 5a) was gradually increased as a function of time, while BOX-decamer aggregate (Figure 5b) and SCoX aggregate (Figure 5c) were not changed significantly. In addition, these two models revealed that the size of aggregates was either sustained or contracted compared to their initial structures.

We found that our MD simulation results (Figures 4 and 5) are in a good accordance with the solvation free energy analysis using DFT calculation, confirming that the rank of hydrophilicity is MOX > BOX > SCoX. Please note that the branch groups determines the hydrophilicity since the backbone is all commonly 2-oxazoline. In addition, from this study, it is inferred that our MD simulation method is able to describe the molecular interactions and corresponding behavior well for further investigation.

3.2. Flory-Huggins interaction parameter

The miscibilities of reactants and products with blocks such as PMOX, PBOX, and PSCoX are assumed to play key roles for implementing the HKR in SCM nanoreactor. The permeation of reactant/product through the micelle consisting of block copolymer chains is affected not only by the miscibility but also by various factors such as the density in the micelle, the concentration gradient and so on. Though, the miscibility as the result of molecular interaction of reactant/product with each block should be carefully investigated to understand the HKR in SCM nanoreactors. For instance, the high solubility of reactants in the polymer phase indicates the high miscibility between two components, meaning that the reactants have enhanced permeation into the micellar structure. Based on this hypothesis, the Flory-Huggins interaction parameters (χ_{AB}) were calculated to assess the molecular interactions of reactants/products with blocks in the micelle in order to understand the experimental results for the HKR in a micelle consisting of block copolymers.[8, 36]

For this calculation, the 2-oxazoline derivatives such as MOX and BOX were polymerized to have 100 repeating units, while SCoX was polymerized to have 30 repeating units, which is due to the relatively small block length of SCoX compared to other two blocks in a micelle as used in the experimental study.[8] Then, mixtures of polymer-reactant and

polymer-product were prepared with various compositions of reactants and products (15 wt%, 45 wt%, and 70 wt%).

The interaction parameters as a function of the weight fractions of reactants or products were used to thoroughly investigate the characteristics of phase segregation with various mixture compositions. As a result, 72 sets of simulations were performed to characterize the compatibility of four reactants and their corresponding products with three polymer blocks. The corresponding number of molecules for each mixture model is listed in Table 4.

Once the initial structures were constructed, first, we ran annealing MD simulations for 8.5 ns, which consists of the heating and cooling processes, to achieve the relaxation of highly strained local structures. The details of the annealing MD simulation is found in the previous publications.[49] Then, an additional 2-ns NVT MD simulation and a subsequent 5-ns NPT MD simulation were performed at 1atm and 300K for equilibration. From the equilibrated systems, the cohesive energy ($\Delta E_{Cohesive}$) was calculated by following equation:

$$\Delta E_{Cohesive} = E_{System} - \sum_i n_i E_i \qquad (4)$$

where E_{System}, n_i, and E_i denote the energy of the system, the number of component molecule, and the energy of a single component molecule, respectively. After converting the weight fraction to the volume fraction, all the variables are substituted into Equation (3) to calculate the Flory-Huggins interaction parameter.

Reac-Cl and Pro-Cl. Figures 6a and 6b shows a series of the χ as a function of the weight fraction of reactant (Reac-Cl) and product (Pro-Cl), respectively. Figure 6a presents that the Reac-Cl has the largest χ value for the corona (PMOX) which keeps increasing with increasing weight fraction of reactant, indicating that that the Reac-Cl would not be well associated with corona (PMOX) of the micelle. Therefore, it is inferred that Reac-Cl would have very poor conversion in this micelle system due to the large χ parameter estimation predicting. Since the χ parameters with PBOX and PSCoX are smaller than that with PMOX, it is anticipated that the Reac-Cl in the corona (PMOX) might have a tendency to move toward to the inner regions of the micelle for better thermodynamic stability.

On the other hand, it is found from Figure 6b that the corresponding product, Pro-Cl has small χ parameter with the core (PSCoX), indicating that the Pro-Cl could stay within the core for a while. However, as the concentration of Pro-Cl increases beyond the weight fraction of 0.6, its χ parameter becomes similar to that in PBOX. Thus, the Pro-Cl would be pushed out of the core. Overall, the reactant would not be able to enter the micelle well and the product would stay long in the micelle, implying that the reaction rate would be low.

Reac-Ph and Pro-Ph. As Figure 7a and 7b, the change of χ parameters for Reac-Ph and Pro-Ph are very similar with the previous case for Reac-Cl and Pro-Cl: it is not easy thermodynamically that the reactant, Reac-Ph gets into the corona of the micelle. Please note in Figure 7a that the χ parameters with the core is relatively small compared to that in the corona, so that the insertion of Reac-Ph into the micelle core seems much easier than that for the case of Reac-Cl. For the Pro-Ph shown in Figure 7b, the curves have similar behavior with those in Figure 6b. Therefore, it is expected that the association of Reac-Ph into the micelle is not thermodynamically easy, which is similar to the case of Reac-Cl. However, the incorporation of reactant into the micelle core would be greater for Reac-Ph than Reac-Cl due to the higher miscibility (smaller χ parameter) with the core.

Reac-C4 and Pro-C4. As can be seen in Figures 8a and 8b, the χ_{AB} parameters of both Reac-C4 and Pro-C4 are smaller than the previous two cases. This means that Reac-C4 and Pro-C4 would be relatively well associated with the blocks in the micelle. Especially, at the weight fraction of ~ 0.45, the solubility of Reac-C4 in each polymer is expected to be relatively favorable for the permeation. Therefore, it is anticipated that the favorable mixing thermodynamics for the reactant-polymer pair would enhance the HKR, which is clearly in a good agreement with the values in Table 1: the time required to complete the HKR is much shorter than the previous two cases. Now, we have one more case: according to the experimental results reported in Table 1, this last reactant has the best HKR efficiency. We see whether or not the rationalization based on χ_{AB} parameters would be valid.

Reac-OPh and Pro-OPh. First, the χ_{AB} parameter of Reac-OPh with the corona (PMOX) is the lowest among the reactants simulated in this study, which facilitates the entrance of Reac-OPh into the micelle. Although the χ_{AB} parameter of Reac-OPh with the PBOX is slightly higher than that of Reac-C4 with the PBOX, the portion of PBOX block in the block copolymer in the experiment[8] is relatively insignificant compared to the portion of PMOX. It

should also be noted that the χ_{AB} parameter with the core (PSCoX) is the lowest among the reactants. From the overall observations from the χ_{AB} parameters, it seems that Reac-OPh would have the most supportive environment in the micelle for the HKR. Furthermore, the miscibility of Pro-OPh with the core is slightly less than those of other products, meaning that, once the HKR reaction occurs, the Pro-OPh would be released out well compared to other products. Indeed, our χ_{AB} parameters for Reac-OPh and Pro-OPh rationalize why the HKR of Reac-OPh proceeds the best compared to other cases.

3.3 Potnetial of Mean Force Analysis

In this study, to validate the conclusions obtained in the previous section, we performed the potential of mean force analysis using steered molecular dynamics (SMD) that canestimate the free energy change as molecule is displaced from solvent phase to polymer phase. Therefore, it was intended that this SMD simulation confirms that the miscibility of the reactant/product with polymers has strong correlation with the reaction rate of HKR.

To calculate the potentials of mean force (PMF), the molecule was displaced through the quasi-static states.[50] For the robust calculation of the PMF, eight sets of SMD simulation were performed independently to obtain an ensemble average of the PMF results by the following definition:

$$PMF(r) = -RT \ln\left[\frac{1}{n}\sum_{i=1}^{n}\exp\left(\frac{-PMF_i(r)}{RT}\right)\right] \quad (5)$$

where R, T, n and r denote the gas constant, temperature, number of trajectories, and displacement coordinate, respectively. Through this procedure, the PMFs were averaged as introduced from the Jarzynski equality that is most frequently used to calculate approximate free energy change over a given irreversible paths. The free energy change is estimated by taking difference in values of PMF between point A and B.

In this study, a single reactant molecule was displaced at the rate of 10^{-5} Å/fs from the water phase to the center of polymer phase (Figure 10). To construct the polymer phase in a slab structure, we prepared the bulk phases of PMOX with the degree of polymerization (DP) of 50 and PSCoX with DP of 15 using NPT MD simulations at 300 K for 3 ns, and then

extended one axis direction to make a slab. For this PMF analysis, we chose Reac-Cl and Reac-OPh because Reac-Cl and Reac-OPh show the least and most miscibility with the PMOX and PSCoX in the previous χ parameter analysis results. The reactant molecule was initially positioned approximately 10~15 Å above from the surface of polymer slab.

The results of the SMD simulations are displayed in Figure 11. According to the profile of PMF and density of polymer in the system, the PMF curves show a noticeable change along the direction of molecule displacement, especially when the reactants enter the polymer phase from the water phase. For both reactant molecules, it is commonly observed that the values of PMF drop at the surface of polymer slab. It is because the reactant molecules are more stable in the polymer phase compared to the water phase. It is also found that the PMF drop for Reac-OPh is ~1.2 kcal/mol and ~1.5 kcal/mol in PMOX (Figure 11a) and PSCoX (Figure 11b), respectively, while that for Reac-Cl is ~0.4 kcal/mol for both polymer phases (Figures 11a and 11b), which means that the free energy stabilization for Reac-OPh is greater when it enters the polymer phase in comparison to Reac-Cl. It is thought that the PMF change of reactants such as Reac-Cl and Reac-OPh is in a good agreement with the conclusion from the χ parameter-based miscibility, confirming that the χ parameter-based miscibility has strong correlation with the reaction rate of HKR.

4. Conclusions

The mixture systems of epoxides and diols with 2-oxazoline-based homopolymers were investigated using MD simulation method, from which the Flory-Huggins interaction parameters (χ) for each system were obtained to evaluate the miscibility of reactant/product with blocks in a micelle. Using these χ parameters, it was found that the molecular miscibility has strong correlation with the reaction rate of HKR in multicompartment micelle. To validate the scheme of the employed MD simulation, the solvation of blocks via MD simulation were compared to the solvation free energy calculated using DFT method with COSMO solvation method. According to the MD simulation results, it was observed that the PMOX oligomers are dispersed from the initial aggregate in water phase whereas the cluster of PBOX and PSCoX stayed as aggregated. The DFT solvation free energy of each block was in a good agreement with the MD simulation, confirming that the MD simulation can describe the interaction of blocks with solvent molecules.

To perform a thorough analysis based on the χ parameters, the blend systems were constructed with various compositions such as 15, 45 and 70 wt% of the reactant/product molecules with respect to the mixed polymers, indicating that the solubility of Reac-OPh in PMOX is the highest among others, followed by Reac-C4, Reac-Ph, and Reac-Cl. To validate these findings, the change of PMF during molecular displacement of Reac-Cl and Reac-OPh into polymer phases such as PMOX and PSCoX was calculated using SMD simulation. The results presented that the decrease of PMF for Reac-OPh is greater than that of Reac-Cl, meaning that the the incorporation of Reac-OPh is graeter than that of Reac-Cl. Overall, it was concluded from our χ parameter calculations that the better miscibility of the reactants with polymer blocks would enhance the higher reaction rate as long as the reactivity is the same.

In the future, the model micelle structure will be investigated to elucidate the radial density distribution of each block in order to quantitatively characterize the reactant/product transport with the actual compositions of the micelle. We believe the spatial distribution of blocks through the micelle will provide more detailed information for molecular diffusion of reactants/products as well as their thermodynamic distributions.

Acknowledgments

This research was supported by the Department of Energy (DE-FG02-03ER15459). We also acknowledge that this research used resources of the Keeneland Computing Facility at the Georgia Institute of Technology, supported by the National Science Foundation under Contract OCI-0910735.

References

1. K. L. Mittal, *Micellization, Solubilization, and Microemulsions*, Springer US, 1 edn., 1977.
2. P. C. Hiemenz, *Principles of Colloid and Surface Chemistry*, Marcell Dekker, INC., New York, 2 edn., 1986.
3. M. Miyamoto, K. Naka, M. Shiozaki, Y. Chujo and T. Saegusa, *Macromolecules*, 1990, **23**, 3201-3205.
4. A. Mero, G. Pasut, L. D. Via, M. W. M. Fijten, U. S. Schubert, R. Hoogenboom and F. M. Veronese, *J. Control. Release*, 2008, **125**, 87-95.
5. M. C. Woodle, C. M. Engbers and S. Zalipsky, *Bioconjugate Chem.*, 1994, **5**, 493-496.
6. S. Zalipsky, C. B. Hansen, J. M. Oaks and T. M. Allen, *J. Pharma. Sciences*, 1996, **85**, 133-137.
7. O. Nuyken, P. Persigehl and R. Weberskirch, *Macromol. Symp.*, 2002, **177**, 163-174.
8. Y. Liu, Y. Wang, Y. Wang, J. Lu, V. Piñón and M. Weck, *J. Am. Chem. Soc.*, 2011, **133**,

14260-14263.
9. Y. Liu, V. Pinon and M. Weck, *Polym. Chem.*, 2011, **2**, 1964-1975.
10. R. J. Hunter and L. R. White, *Foundations of colloid science*, Clarendon Press, 1987.
11. F. Reiss-Husson and V. Luzzati, *J. Phys. Chem.*, 1964, **68**, 3504-3511.
12. N. A. Mazer, G. B. Benedek and M. C. Carey, *J. Phys. Chem.*, 1976, **80**, 1075-1085.
13. C. Y. Young, P. J. Missel, N. A. Mazer, G. B. Benedek and M. C. Carey, *J. Phys. Chem.*, 1978, **82**, 1375-1378.
14. A. Rohde and E. Sackmann, *J. Colloid Interf. Sci.*, 1979, **70**, 494-505.
15. P. J. Missel, N. A. Mazer, G. B. Benedek, C. Y. Young and M. C. Carey, *J. Phys. Chem.*, 1980, **84**, 1044-1057.
16. R. J. Hunter, *Foundations of Colloid Science*, Clarendon Press, Oxford, 1986.
17. V. Sfika, C. Tsitsilianis, A. Kiriy, G. Gorodyska and M. Stamm, *Macromolecules*, 2004, **37**, 9551-9560.
18. F. Wiesbrock, R. Hoogenboom, M. A. M. Leenen, M. A. R. Meier and U. S. Schubert, *Macromolecules*, 2005, **38**, 5025-5034.
19. H. Schlaad, C. Diehl, A. Gress, M. Meyer, A. L. Demirel, Y. Nur and A. Bertin, *Macromol. Rapid Commun.*, 2010, **31**, 511-525.
20. P. Persigehl, R. Jordan and O. Nuyken, *Macromolecules*, 2000, **33**, 6977-6981.
21. T. Kotre, M. T. Zarka, J. O. Krause, M. R. Buchmeiser, R. Weberskirch and O. Nuyken, *Macromol. Symp.*, 2004, **217**, 203-214.
22. M. Tokunaga, J. F. Larrow, F. Kakiuchi and E. N. Jacobsen, *Science*, 1997, **277**, 936-938.
23. J. F. Larrow and E. N. Jacobsen, *Organic Syntheses, Vol 75*, 1998, **75**, 1-11.
24. A. Klamt and G. Schuurmann, *J. Chem. Soc., Perkin Trans. 2*, 1993, DOI: 10.1039/P29930000799, 799-805.
25. C. F. Fan, B. D. Olafson, M. Blanco and S. L. Hsu, *Macromolecules*, 1992, **25**, 3667-3676.
26. M. Doi, *Introduction to Polymer Physics*, Clarendon Press, 1996.
27. K. Pajula, M. Taskinen, V.-P. Lehto, J. Ketolainen and O. Korhonen, *Mol. Pharm.*, 2010, **7**, 795-804.
28. T.-X. Xiang and B. D. Anderson, *Mol. Pharm.*, 2012, **10**, 102-114.
29. A. O. Kasimova, G. M. Pavan, A. Danani, K. Mondon, A. Cristiani, L. Scapozza, R. Gurny and M. Möller, *J. Phys. Chem. B*, 2012, **116**, 4338-4345.
30. S. Thakral and N. K. Thakral, *J. Pharma. Sciences*, 2013, **102**, 2254-2263.
31. J. S. Patel, A. Berteotti, S. Ronsisvalle, W. Rocchia and A. Cavalli, *J. Chem. Inf. Model.*, 2014, **54**, 470-480.
32. J. Siepmann, F. Lecomte and R. Bodmeier, *J. Control. Release*, 1999, **60**, 379-389.
33. X. D. Guo, J. P. K. K. Tan, S. H., L. J. Zhang, Y. Zhang, J. L. Hedrick, Y. Y. Yang and Y. Qian, *Biomaterials*, 2009, **30**, 6556-6563.
34. V. Vivcharuk and Y. N. Kaznessis, *J. Phys. Chem. B*, 2011, **115**, 14704-14712.
35. X. D. Guo, Y. Qian, C. Y. Zhang, S. Y. Nie and L. J. Zhang, *Soft Matter*, 2012, **8**, 9989-9989.
36. M. Paloncýová, K. Berka and M. Otyepka, *J. Chem. Theory Comput.*, 2012, **8**, 1200-1211.
37. S. M. Loverde, *J. Phys. Chem. Lett.*, 2014, **5**, 1659-1665.
38. S. Patel, A. Lavasanifar and P. Choi, *Biomacromolecules*, 2008, **9**, 3014-3023.
39. A. O. Kasimova, G. M. Pavan, A. Danani, K. Mondon, A. Cristiani, L. Scapozza, R. Gurny and M. Möller, *J. Phys. Chem. B*, 2012, **116**, 4338-4345.
40. M. T. Zarka, O. Nuyken and R. Weberskirch, *Chem. Eur. J.*, 2003, **9**, 3228-3234.
41. S. L. Mayo, B. D. Olafson and W. A. Goddard, *J. Phys. Chem.*, 1990, **94**, 8897-8909.
42. R. S. Mulliken, *J. Chem. Phys.*, 1955, **23**, 1833-1840.

43. A. D. Bochevarov, E. Harder, T. F. Hughes, J. R. Greenwood, D. A. Braden, D. M. Philipp, D. Rinaldo, M. D. Halls, J. Zhang and R. A. Friesner, *Int. J. Quantum Chem.*, 2013, **113**, 2110-2142.
44. S. Nosé, *J. Chem. Phys.*, 1984, **81**, 511-519.
45. W. G. Hoover, *Phys. Rev. A*, 1985, **31**, 1695-1697.
46. R. W. Hockney and J. W. Eastwood, *Computer Simulation Using Particles*, Taylor & Francis, Inc., 1988.
47. W. C. Swope, H. C. Andersen, P. H. Berens and K. R. Wilson, *J. Chem. Phys.*, 1982, **76**, 637-649.
48. S. Plimpton, *J. Comput. Phys.*, 1995, **117**, 1-19.
49. S. S. Jang, V. Molinero, T. Çağın and W. A. Goddard, *J. Phys. Chem. B*, 2004, **108**, 3149-3157.
50. S. Park and K. Schulten, *J. Chem. Phys.*, 2004, **120**, 5946-5961.

Table 1. Summary of the HKR of epoxides and experimental results using SCM catalyst **5**

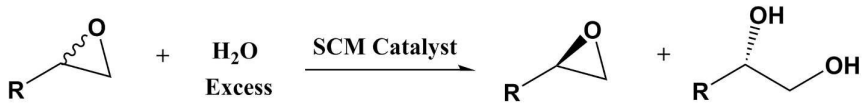

Entry[a]	Reactant (epoxide)	Product (diol)	R	Time (h)[b]	Conv. (%)
1	Epichlorohydrin (Reac-Cl)	Chloropropane diol (Pro-Cl)	CH_2Cl	24	4
2	Styrene oxide (Reac-Ph)	Phenylethane diol (Pro-Ph)	Ph	12	48
3	Epoxyhexane (Reac-C4)	Hexane diol (Pro-C4)	*n*-butyl	8	50
4	Phenyl glycidyl ether (Reac-OPh)	Phenol glycerol ether (Pro-OPh)	CH_2OPh	5	49

[a] The reactions were carried out at room temperature using SCM catalyst **5** with a 0.1 mol% catalyst loading.
[b] The time required to complete the HKR of epoxide.

Table 2. Specifications of simulated models in DFT calculation

Species	DP*	Surface Area (Å²)	
		Monomer	Oligomer
Octamer of 2-methyl-2-oxazoline (MOX)	8	62.70	238.35
Tetramer of 2-(3-butinyl)-2-oxazoline (BOX)	4	89.65	237.49
Co(III)-salen (SCoX) attached with methyl-3-(oxazol-2-yl)pentanoate	1	262.45	-

*DP denotes the degree of polymerization or number of repeating units in oligomer

Table 3. Conditions of the MD simulation for the cluster of oligomers in the water phase

	MOX	**BOX**	**SCoX**
Final Density of System	1.002±0.002	1.001±0.001	1.001±0.002
Weight Fraction of Solute	5.3 wt%	3.7 wt%	3.8 wt%
Number of oligomers per Cluster		15	

Table 4. Content information of reactants and products in the mixture

Polymer Block	Terminal (R in Table 1)	Number of Molecules in the Mixture with Polymer (corresponding volume fraction in %)							
		Cl (Cl)		Phenyl (Ph)		C_4H_9 (C4)		CH_2OPh	
	Weight Fraction	Reactant	Product	Reactant	Product	Reactant	Product	Reactant	Product
PSCoX	15%	100(17)	68(7)	80(11)	55(7)	55(7)	50(8)	68(7)	60(6)
	45%	400(46)	317(39)	380(50)	254(39)	254(39)	227(38)	317(39)	276(37)
	70%	1200(69)	900(68)	1080(73)	723(69)	723(69)	380(68)	900(68)	790(67)
PMOX	15%	16(15)	12(11)	15(15)	10(11)	10(11)	9(10)	12(11)	11(10)
	45%	75(45)	58(42)	70(52)	47(42)	47(42)	41(40)	58(42)	50(40)
	70%	220(68)	165(69)	200(76)	132(68)	132(68)	120(68)	165(69)	144(67)
PBOX	15%	24(15)	18(13)	20(16)	15(13)	15(13)	15(14)	18(13)	16(11)
	45%	110(44)	84(44)	100(52)	67(43)	67(43)	60(42)	84(44)	73(42)
	70%	310(66)	240(70)	290(77)	191(69)	191(69)	170(54)	240(70)	208(69)

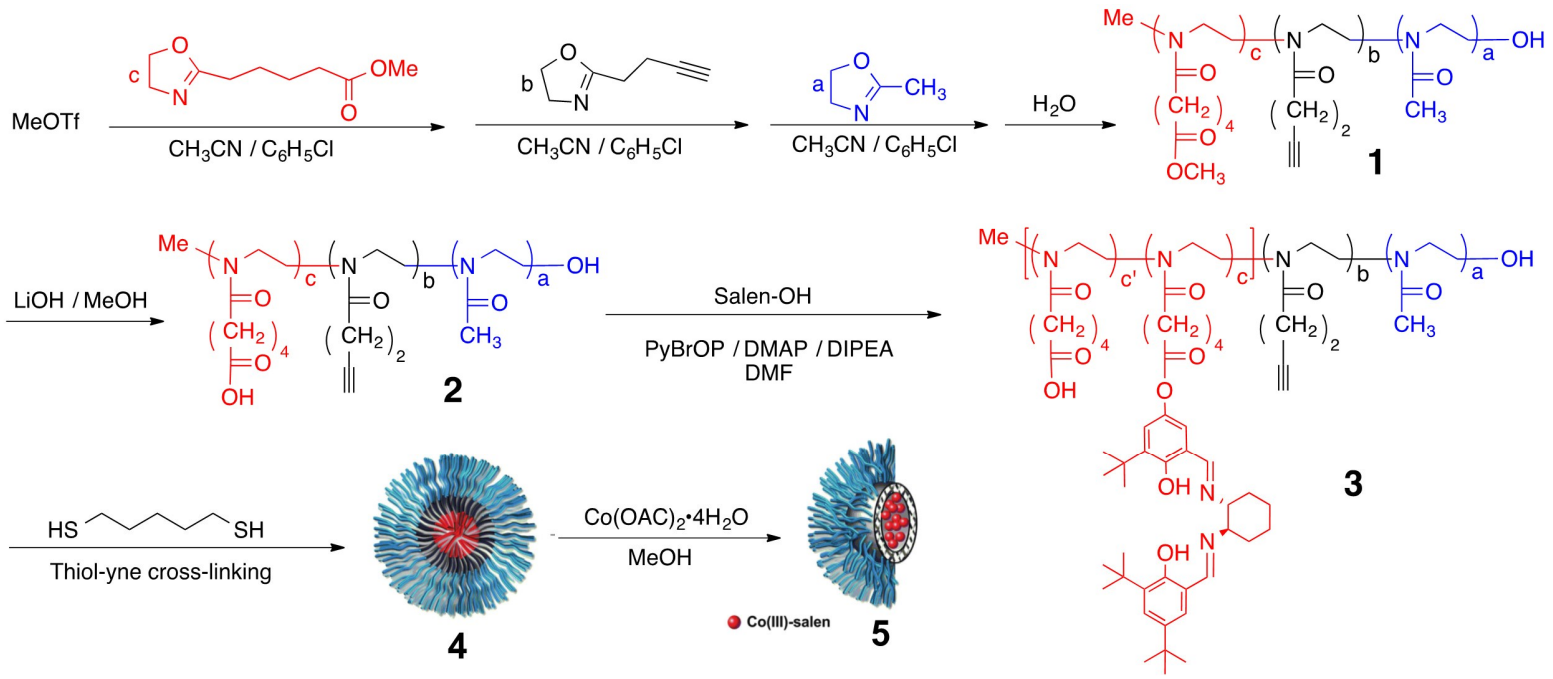

Scheme 1. Schematic representation of the synthesis of poly(2-oxazoline) SCM with Co(III)-salen in the micelle core.

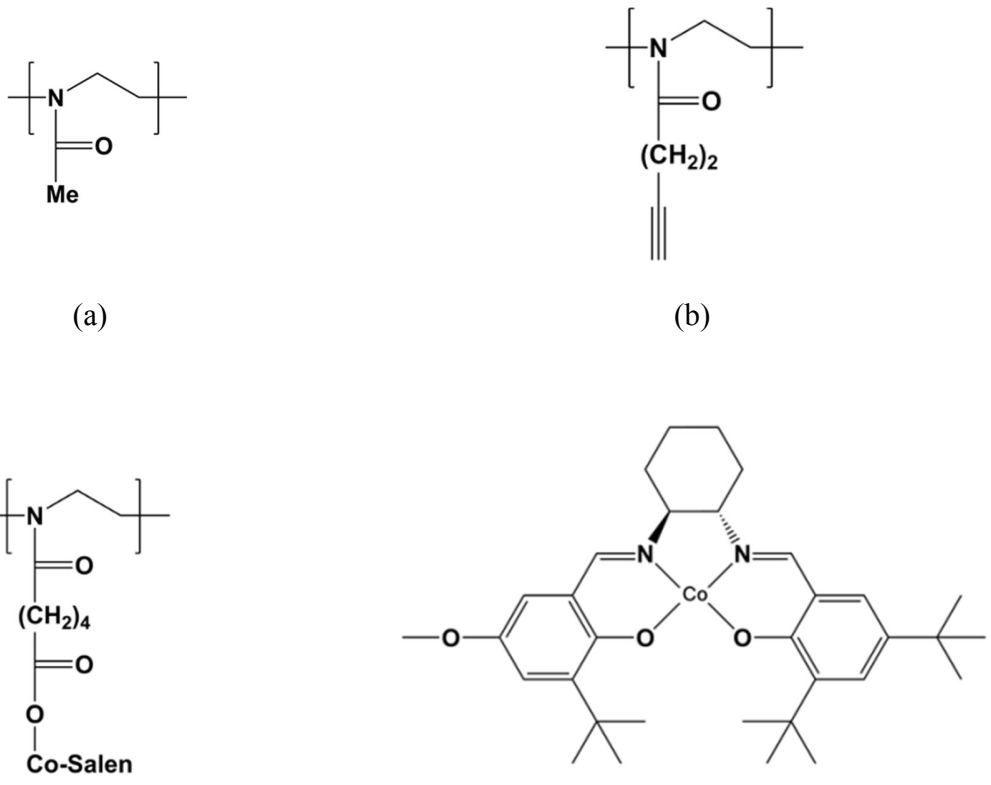

Figure 1. Monomers used in this study: (a) poly(2-methyl-2-oxazoline) (PMOX); (b) poly(2-(3-butinyl)-2-oxazoline) (PBOX); and (c) poly(methyl-3-oxazol-2-yl) pentanoate with (d) Co(III)-salen (PSCoX).

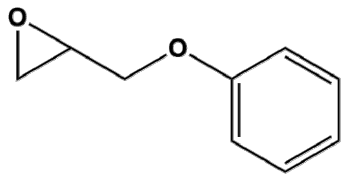

(a)

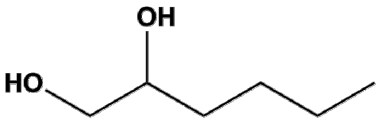

(b)

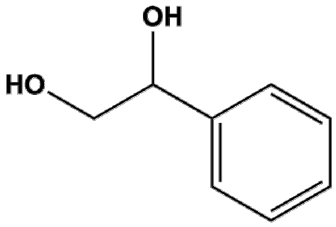

(c)

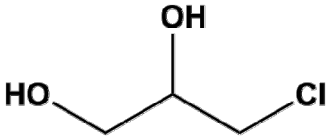

(d)

Figure 2. Chemical structures of the tested reactants and products. The left side of the figure contains the chemical structures of the reactants while the products are listed on the right side. (a) phenyl glycidyle ether and phenol glycerol ether (R-OPh and P-OPh) (b) epoxyhexane and hexane diol (R-C4 and P-C4) (c) styrene oxide and phenylethane diol (R-Ph and P-Ph) (d) epichlorohydrine and chloropropane diol (R-Cl and P-Cl).

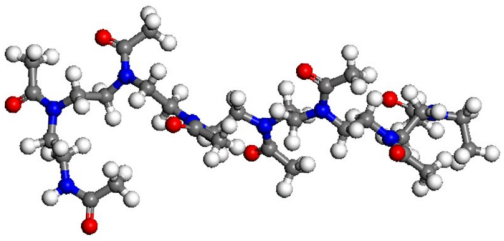

(a)

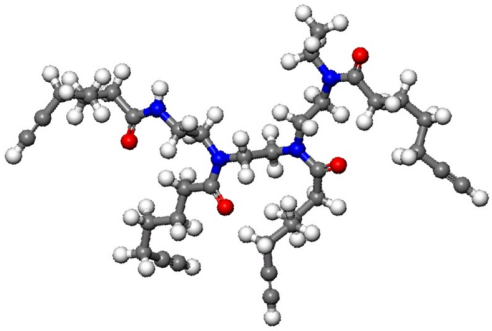

(b)

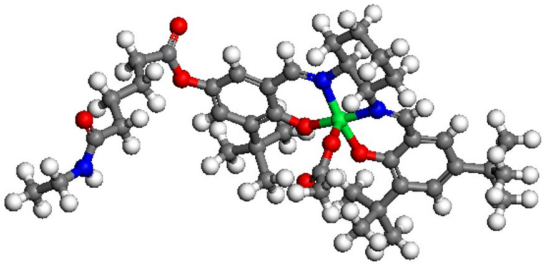

(c)

Figure 3. Molecules used in the DFT calculation: (a) octamer of 2-methyl-2-oxazoline; (b) tetramer of 2-(3-butinyl)-2-oxazoline; (c) Co(III)-salen attached with methyl-3-(oxazol-2-yl)pentanoate.

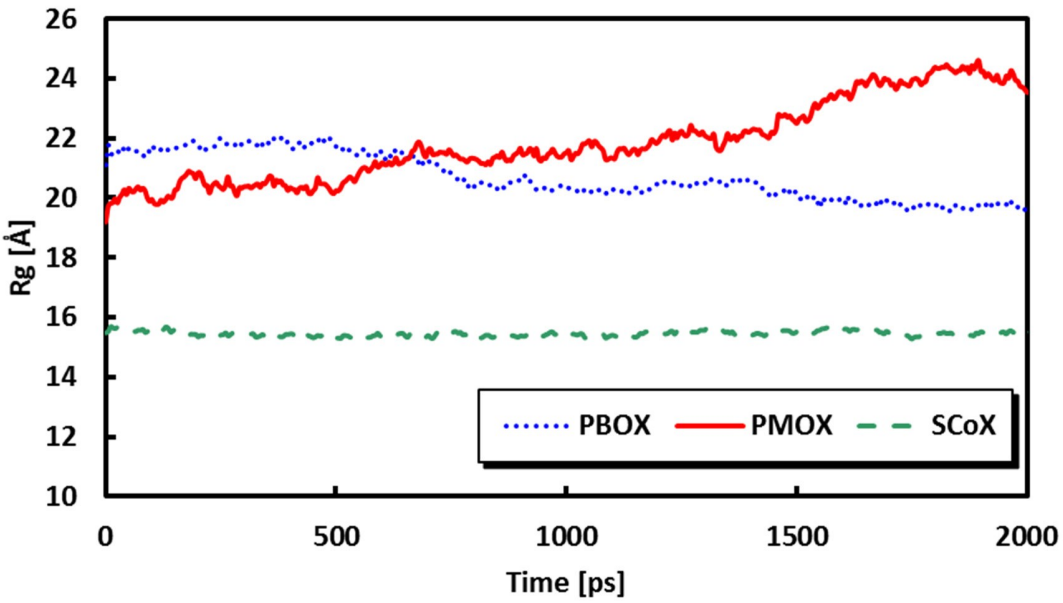

Figure 4. Change in the radius of gyration of molecular aggregates during 2 ns of NPT-MD simulation.

Initial Final

(a)

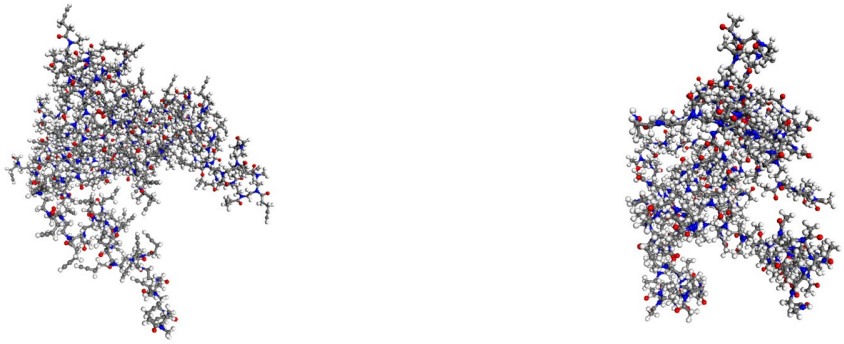

Initial Final

(b)

Initial Final

(c)

Figure 5. Snapshot of the cluster structures via 2ns-NPT MD simulations: (a) PMOX; (b) PBOX; (c) SCoX. The water molecules are invisible for clear view.

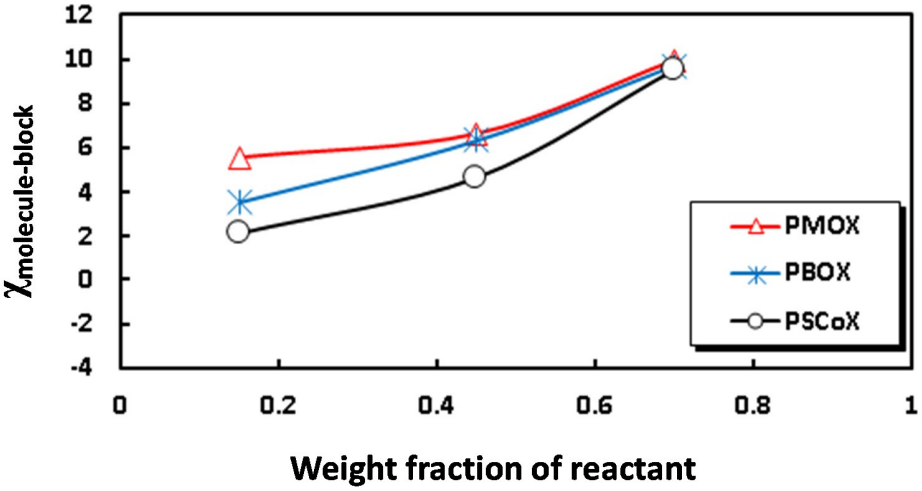

(a)

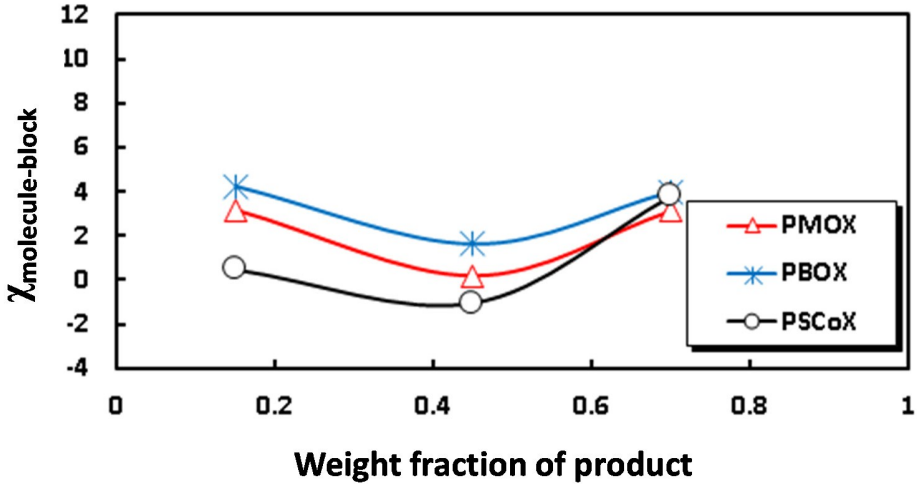

(b)

Figure 6. Change of $\chi_{molecule\text{-}block}$ calculated from mixture of block with (a) Reac-Cl and (b) Pro-Cl with blocks, as a function of weight fraction of molecules.

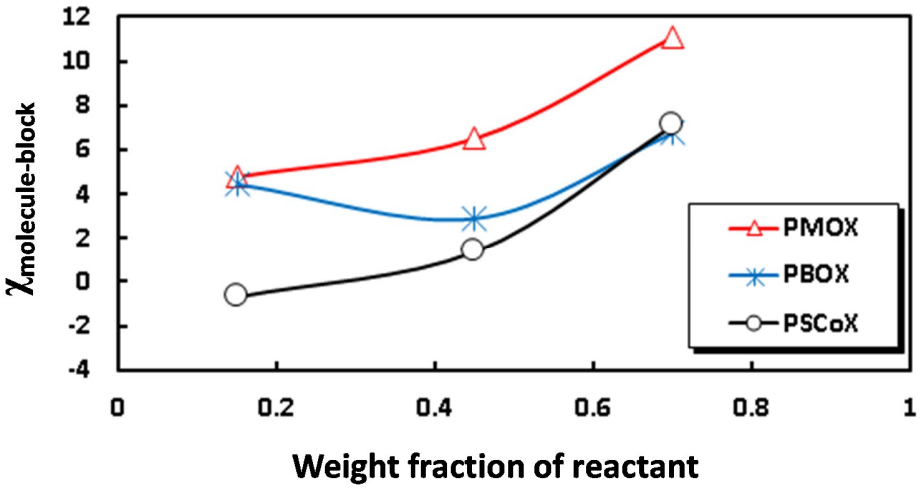

(a)

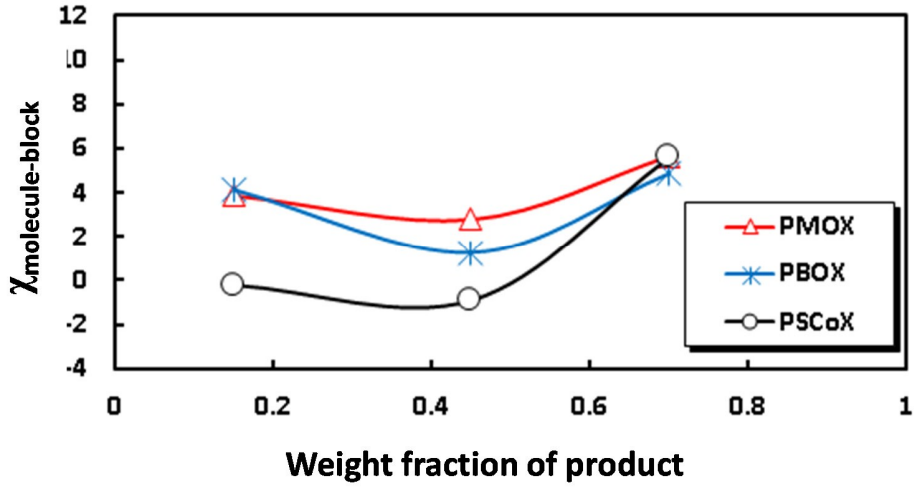

(b)

Figure 7. Change of $\chi_{molecule\text{-}block}$ calculated from mixture of block with (a) Reac-Ph and (b) Pro-Ph with blocks, as a function of weight fraction of molecules.

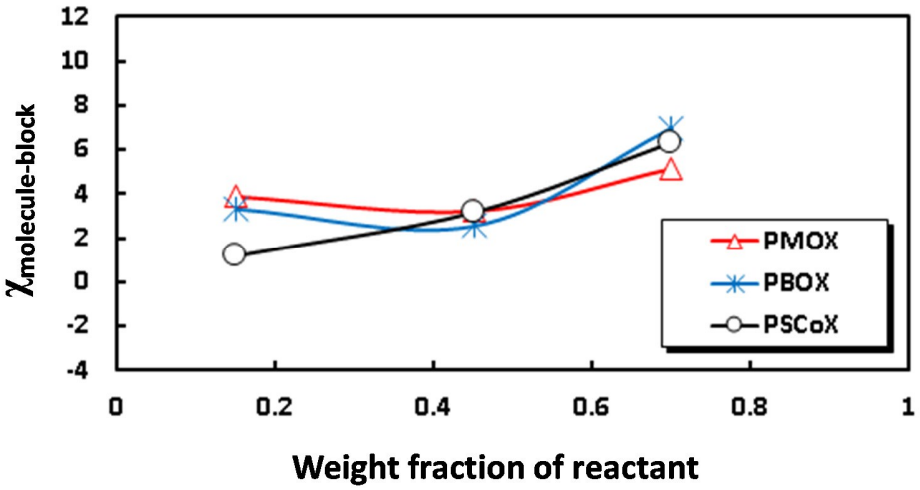

(a)

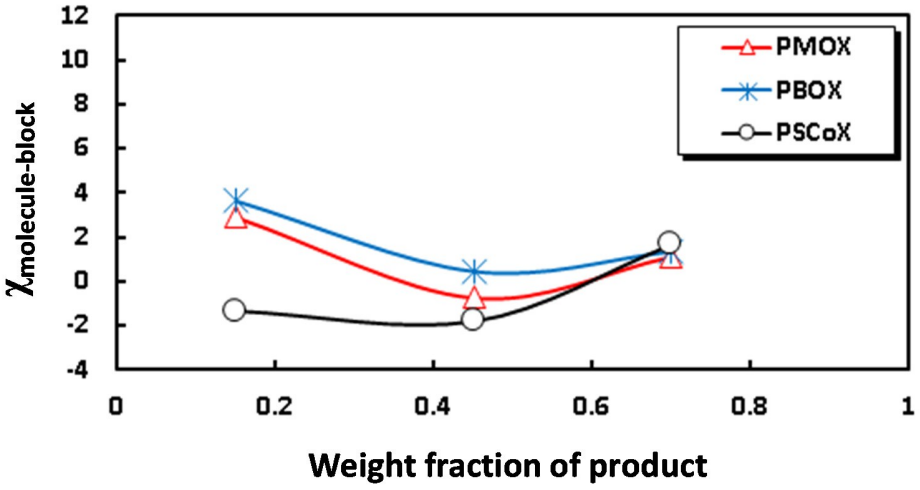

(b)

Figure 8. Change of $\chi_{molecule\text{-}block}$ calculated from mixture of block with (a) Reac-C4 and (b) Pro-C4 with blocks, as a function of weight fraction of molecules.

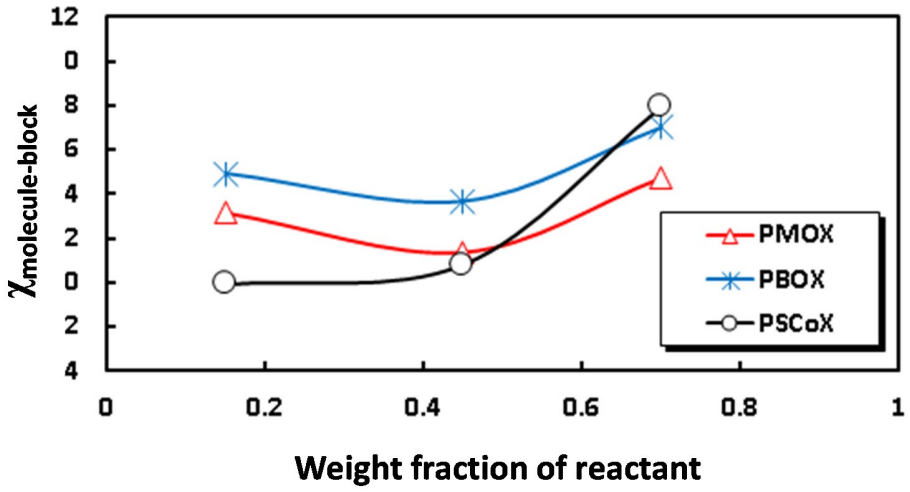

(a)

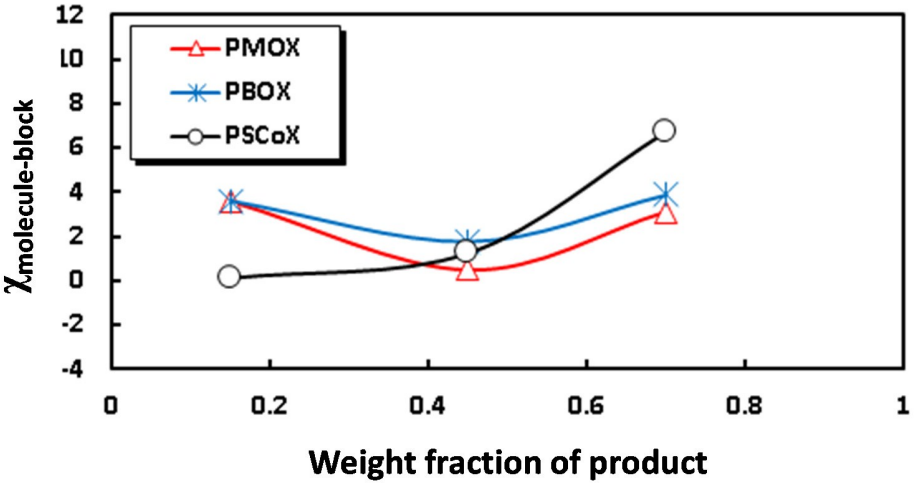

(b)

Figure 9. Change of $\chi_{molecule\text{-}block}$ calculated from mixture of block with (a) Reac-OPh and (b) Pro-OPh with blocks, as a function of weight fraction of molecules.

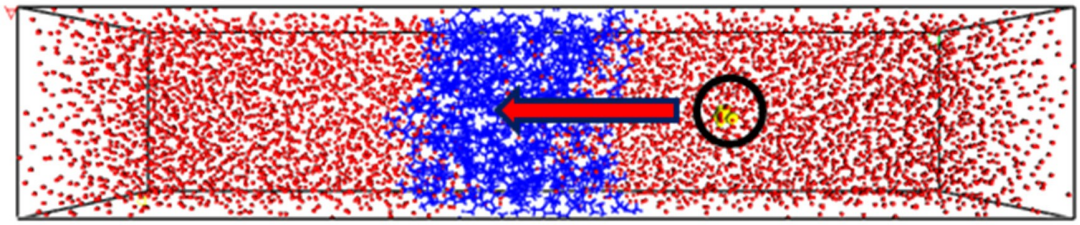

Figure 10. Scheme of steered molecular dynamics simulation. Black circle and red arrow indicate the initial position of reactant molecule and the direction of the displacement, respectively. Red and blue color denote the water molecules and polymers, respectively.

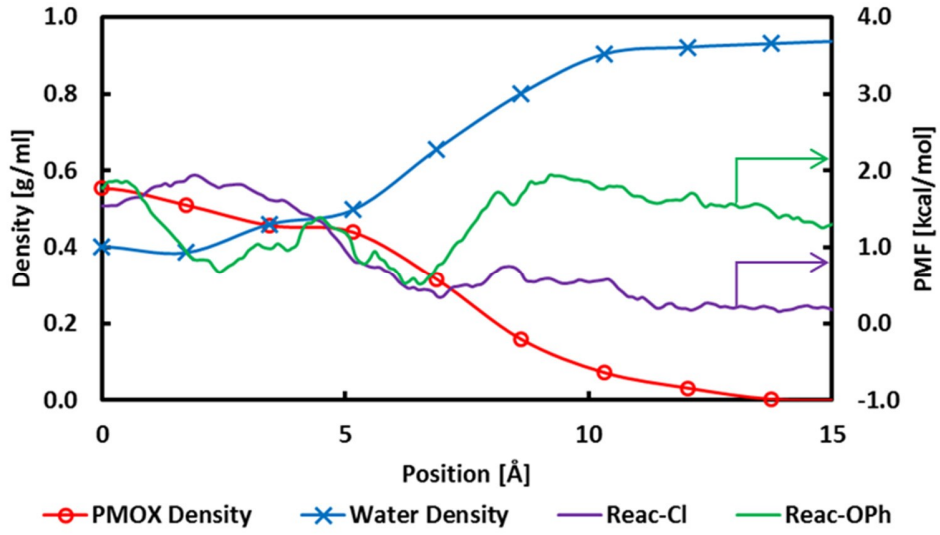

(a)

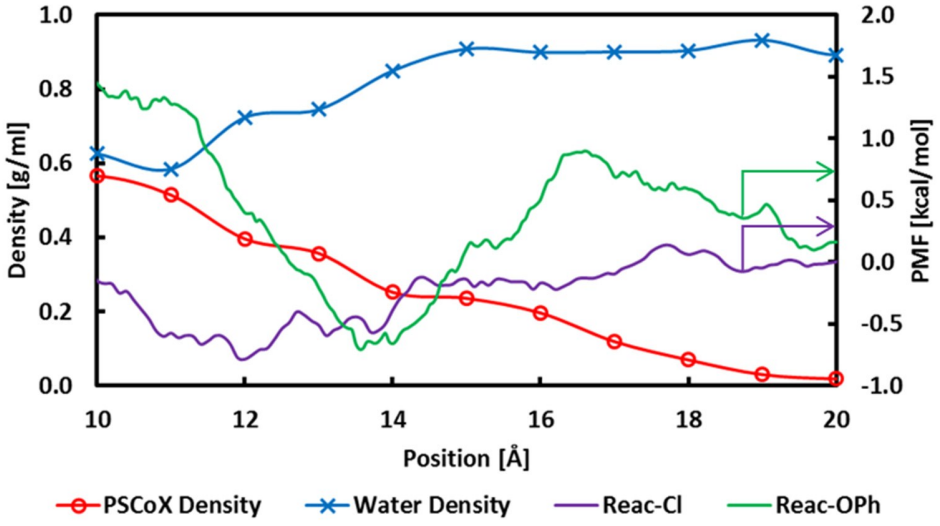

(b)

Figure 11. Profiles of density and potentials of mean force as a function of position: Polymer slabs are (a) PMOX and (b) PSCoX.